Optomechanical nanoantenna

Alireza Bonakdar, John Kohoutek, Dibyendu Dey, and Hooman Mohseni*

Bio-inspired Sensors and Optoelectronics Laboratory (BISOL), Department of Electrical Engineering and Computer Science, Northwestern University, Evanston, Illinois 60208, USA
**Corresponding author: hmohseni@northwestern.edu*

Received March 22, 2012; revised May 25, 2012; accepted June 22, 2012;
posted June 26, 2012 (Doc. ID 164510); published July 30, 2012

We introduce optomechanical nanoantennae, which show dramatic changes in scattering properties by minuscule changes in geometry. These structures are very compact, with a volume 500 times smaller than free-space optical wavelength volume. This deep subwavelength geometry leads to high speed and low switching power. The bandwidth of the device is about 4.4 GHz, with a switching energy of only 35 pJ. Such antenna structures could lead to compact and high-speed all-optical nanoswitches. © 2012 Optical Society of America

OCIS codes: 230.4110, 250.5403, 250.6715, 130.4815, 230.0230, 250.5300.

The principle of surface plasmon polariton (SPP) has been exploited by many research groups to achieve high speed and compact nanoswitches, for example, tuning the SPP wavelength by controlling the refractive index of the substrate of a nanoantenna [1]. Recent development of plasmonic nanoswitches includes gap-loading approaches, where the gap region of the coupled nanoantenna is loaded with photoconductive [2], nonlinear [3], or anisotropic material [4]. Thus, the scattering response of a nanoantenna can be changed strongly by controlling the dielectric property of the material in the antenna gap [5–7].

An optomechanical nanoantenna could be defined as a type of optical antenna that is mechanically reconfigured by the near-field optical force. Thus, the scattering properties of the antenna can be dynamically controlled without requiring any material in the antenna gap. The force density that is localized to a subwavelength area is very large [8], as we have also recently verified experimentally [9]. Here, we present an example of an optomechanical nanoantenna that utilizes these features to achieve unprecedented performance. The device is composed of a plasmonic bowtie antenna with suspended curved beams attached to the end of each arm, as shown in Fig. 1(a). The antenna structure is considered to be made of aluminum, where the length of the antenna is 170 nm with 40 nm thickness. Since selective anisotropic etching of the substrate could release narrow components due to undercut, a 25 nm depth of etch of the substrate and 25 nm undercut of the antenna were assumed in the simulation. The suspended beams act as movable components of the antenna setup. These create an open oval ring with small air gap regions at the top and bottom of the ring. The minor (along x direction) and major (along y direction) diameters of the elliptical opening were kept fixed at 100 nm and 440 nm, respectively, with a beam width of 40 nm. A 2 nm naturally formed aluminum oxide over all aluminum surfaces was assumed in our simulation. The bowtie antenna provides efficient coupling between the free-space optical source with polarization along the antenna long axis, and it generates a strong optical near field in the gap regions of the antenna. The near-field intensity profile at 25 nm above the antenna surface is also presented in Fig. 1(a). The gradient of the confined optical field results in strong optical force between the ends of the curved beams and bends them toward each other [10].

Finite-difference time-domain (FDTD) simulation is used to simulate the antenna structure. Maxwell's stress tensor formulism is applied to calculate generated optical force [9] between the two beams. The optical force along the x axis is attractive and dominant, compared with the other components, as shown in Fig. 1(b). All forces are normalized with respect to a source intensity of 1 mW/μm^2. The Casimir force between two beams [inset in Fig. 1(b)] is also calculated based on the transfer matrix approach for a multilayer system described in [11].

The power transmission and reflection spectrums for the structure are shown in Figs. 1(c) and 1(d) with a redshift due to decreasing gap width. The reflected power (R) is calculated on a 2π hemisphere at the back of the optical source. The transmitted power (T) is derived by calculating the power lost (L) in the device and using the power conservation law $T = 1 - R - L$. The nanoantenna can be considered as a lump element as shown in Fig. 1(e), with impedance $Z_a = R_a + i\omega L_a$ in parallel

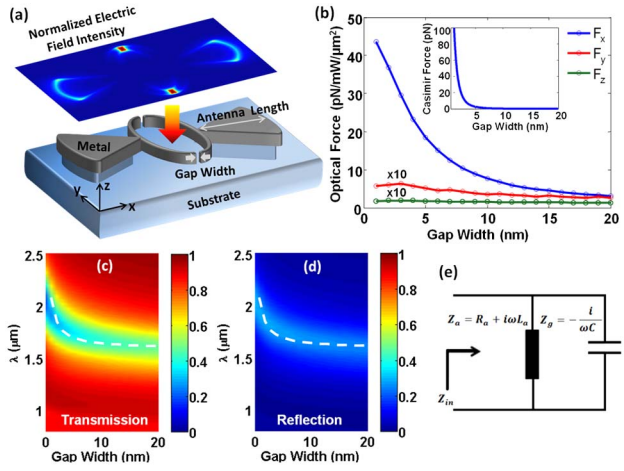

Fig. 1. (Color online) (a) Schematic diagram of the designed optomechanical nanoantenna. The near-field intensity profile of the antenna is shown on top of the 3D view. (b) Simulated optical force on suspended beam as a function of gap; inset, Casimir force as a function of gap. (c) Simulated power transmission and (d) reflection spectrums versus gap width. (e) Nanocircuit lump element model.

with an equivalent capacitor. The equivalent capacitor is composed of the gap capacitor between the suspended beams $Z_g = -i/\omega C_g$ in parallel with the fringe capacitor C_f. The optical resonance frequency of the antenna can be determined by setting the reactive part of the input impedance to be zero, yielding $\omega = 1/\sqrt{L_a(C_g + C_f)}$. The redshift trend in both plots is fitted well by white dashed curves using the resonant frequency formula of the nanocircuit model [Fig. 1(e)]. Such a strong change in antenna scattering due to deep subwavelength gap variation has been experimentally verified [12].

The mechanical behavior of the antenna is analyzed based on the Euler–Bernoulli beam deflection method [13]. For a single-sided clamped beam (cantilever) with a point force (F) exerted at the free end, the beam deflection can be calculated by $\Delta\delta = F/\kappa$, where $\kappa = Etw^3/4L^3$ is the spring constant of the beam with length L and width w. E is Young's modulus, which is 69 GPa for aluminum, tw^3 is proportional to the second momentum of area for a beam with rectangular cross section. In addition, the mechanical resonant frequency of a single-sided and double-sided clamped beam can be calculated by $f_{\text{res}} = A\sqrt{Et^2/\rho L^4}$, where A is the clamping coefficient and ρ is beam density. Thus, the mechanical resonance frequency is inversely proportional to the structure's linear dimension. The size of the optical device could be reduced to subwavelength dimensions by SPP, and as a result, high mechanical frequency is achievable. The proposed device has a mechanical bandwidth of about 4.4 GHz, which is 2 orders of magnitude higher than the natural frequency in conventional optomechanical devices [14,15].

In order to investigate the switching characteristics of the device, Eq. (1) has been solved self-consistently:

$$\delta = \delta_0 - 2\kappa^{-1}(F_{\text{Optical}}(\delta) + F_{\text{Casimir}}(\delta)) \tag{1}$$

where $\delta_0 = 10$ nm is the gap width at zero source illumination. Since the calculated optical force is normalized to source intensity, the gap width solution can be expressed in terms of optical source intensity. Figure 2(a) shows the gap width solutions as a function of optical source intensity and optical wavelength. The minimum switch power is found at an optical wavelength of 1.78 μm. The map of the solution (gap width versus source intensity) for this wavelength is shown in Fig. 2(b). The graph consists of the stable (green line) and unstable (black line) branches. The origin of the unstable/stable condition is the relative magnitude of the mechanical force, which has the opposite direction compared with the optical and Casimir forces. The stable branch results from negative feedback: any infinitesimal change in gap width will change the forces' magnitude to oppose the gap change. In contrast, the unstable branch results from positive feedback. By increasing the source intensity [forward switching—red path in Fig. 2(b)], the width of the gap decreases monotonically, until a critical gap width where the two stable and unstable branches meet each other. At the critical point, any increase in source intensity results in a positive feedback since reduced gap width leads to an increased optical force. Thus, the feedback generates a sudden decrease in gap width from the critical point. As

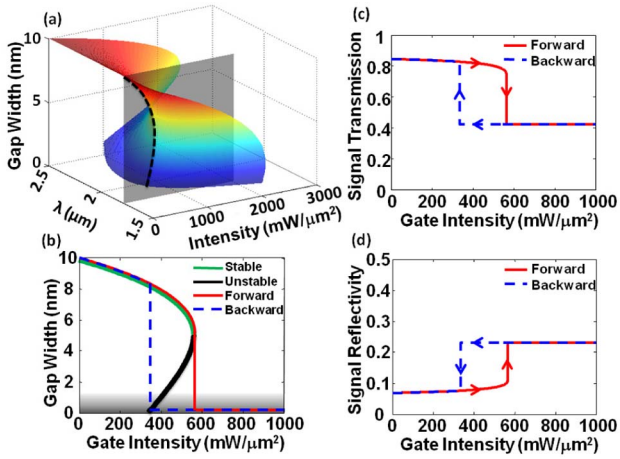

Fig. 2. (Color online) (a) 3D map showing the change in gap width with optical source intensity at different wavelengths. The minimum power required for changing gap width is $\lambda = 1.78$ μm. (b) The minimum power from (a) is redrawn with its stable and unstable branches. (c) Transmission and (d) reflection of signal at $\lambda = 2.04$ μm is controlled by the gate at $\lambda = 1.78$ μm with 4 dB (transmission) and 5 dB (reflectivity) depth of modulations.

the gap approaches a subnanometer width, the electric field intensity and optical force *decrease*. This phenomenon has been investigated earlier [16], and is due to quantum mechanical effects. Thus, the positive feedback mechanism mentioned above gradually decreases in the subnanometer region, resulting in another stable point. This region is shown by a grayed area in Fig. 2(b). For the backward switching (dashed blue path), the gap remains within the grayed area (subnanometer) until the backward path crosses the unstable route where the gate intensity results in an optical force, which in summation with Casimir force cannot withstand the mechanical force required for beam deflection. Thus, there is a sudden jump to the larger gap width in the stable branch where the optical force can keep the beams bent. Further reduction of optical power will decrease the force and the gap width increases. Although the optical source intensity generates a strong force at bistable points where the optical force is 2 orders of magnitude larger than the Casimir force, the role of the Casimir force becomes substantial for small gate source powers where it is comparable with the optical force.

The depth of modulation (DM) of power reflection R and transmission T spectrums are defined by the following expressions:

$$\text{DM}_R = 10 \log \frac{R_{\delta=10\text{ nm}}}{R_{\delta=1\text{ nm}}}, \tag{2a}$$

$$\text{DM}_T = 10 \log \frac{T_{\delta=10\text{ nm}}}{T_{\delta=1\text{ nm}}}, \tag{2b}$$

The optical signal wavelength at 2.04 μm has the largest DM_R (~5 dB). The criteria for choosing the signal wavelength could also be based on DM_T if transmission signal carries information. Therefore, the transmission and

reflection of input signal operating at 2.04 μm can be efficiently controlled by a gate beam operating at 1.78 μm. Figures 2(c) and 2(d) show the switching of the transmission and reflection of the signal controlling the gate intensity for forward and backward switching. The depth of modulation was found to be 4 dB in transmission, and 5 dB in reflection mode. The energy per switch is calculated by multiplication of optical source intensity at abrupt change in forward path, bandwidth, and device area. The energy per switch is found to be 35 pJ due to the small area and high speed of the switch. The wide hysteresis loop ensures robust operation of the switching logic against noise [17]. The thermal analysis of the structure due to optical loss in the antenna is performed by considering the conductive and radiative heat transfer mechanisms and utilizing a thermal equivalent circuit. We took into account the emissivity of the antenna in radiative process, which can modify the blackbody radiation spectrum. Our simulation shows that the resulting temperature increase at the gap between two beams is around 140 K above ambient, which should not affect the overall device performance significantly.

In conclusion, we have demonstrated a new optomechanical nanoantenna structure that can operate as a switch by changing the power transmission and reflection due to a nanometer-scale mechanical reconfiguration caused by generated optical force. In general, we conclude that an efficient optomechanical antenna design should satisfy three conditions: efficient far-field to near-field coupling, strong confinement of light into a subwavelength region to produce considerable optical force, and high sensitivity of the optical response to mechanical deformation. FDTD simulation of electromagnetic fields and Euler–Bernoulli beam deflection theory were applied to calculate switching characteristics of the proposed device. Nanocircuit theory was applied to analyze the near-field properties due to reconfiguration. The presented nanoswitch has high speed (~4.4 GHz), ultracompactness ($\sim\lambda^3/500$), and efficient switching energy (~35 pJ) which results in superior performance when compared with previous optomechanical switches. Such optomechanical devices could be utilized in many novel applications, such as all-optical switches, wavelength mixing, wavelength converters, and other building blocks of photonic integrated circuits.

This work was supported in part by the United States National Science Foundation (CBET-0932611) and United States Army Research Office (USARO) (W911NF-11-1-0390).

References

1. M. Abb, P. Albella, J. Aizpurua, and O. L. Muskens, Nano Lett. **11**, 2457 (2011).
2. N. Large, M. Abb, J. Aizpurua, and O. L. Muskens, Nano Lett. **10**, 1741 (2010).
3. P.-Y. Chen, M. Farhat, and A. Alù, Phys. Rev. Lett. **106**, 105503 (2011).
4. J. Berthelot, A. Bouhelier, C. Huang, J. r. m. Margueritat, G. r. Colas-des-Francs, E. Finot, J.-C. Weeber, A. Dereux, S. Kostcheev, H. I. E. Ahrach, A.-L. Baudrion, J. Plain, R. Bachelot, P. Royer, and G. P. Wiederrecht, Nano Lett. **9**, 3914 (2009).
5. A. Alù and N. Engheta, Phys. Rev. B **78**, 195111 (2008).
6. M. Schnell, A. Garcia Etxarri, A. J. Huber, K. Crozier, J. Aizpurua, and R. Hillenbrand, Nat. Photon. **3**, 287 (2009).
7. A. Alu and N. Engheta, Nat. Photon. **2**, 307 (2008).
8. X. Yang, Y. Liu, R. F. Oulton, X. Yin, and X. Zhang, Nano Lett. **11**, 321 (2011).
9. J. Kohoutek, D. Dey, A. Bonakdar, R. Gelfand, A. Sklar, O. G. Memis, and H. Mohseni, Nano Lett. **11**, 3378 (2011).
10. J. D. Jackson, *Classical Electrodynamics* (Hamilton Printing, 1998).
11. V. A. Parsegian, *Van Der Waals Forces, A Handbook for Biologists, Chemists, Engineers, and Physicists* (Cambridge University, 2006).
12. J. Merlein, M. Kahl, A. Zuschlag, A. Sell, A. Halm, J. Boneberg, P. Leiderer, A. Leitenstorfer, and R. Bratschitsch, Nat. Photon. **2**, 230 (2008).
13. W. T. Weaver, S. P. Timoshenko, and D. H. Young, *Vibrations Problems in Engineering* (Wiley, 1990).
14. D. Van Thourhout and J. Roels, Nat. Photon. **4**, 211 (2010).
15. M. Eichenfield, R. Camacho, J. Chan, K. J. Vahala, and O. Painter, Nature **459**, 550 (2009).
16. J. Zuloaga, E. Prodan, and P. Nordlander, Nano Lett. **9**, 887 (2009).
17. S. Reitzenstein, L. Worschech, P. Hartmann, and A. Forchel, Appl. Phys. Lett. **82**, 1980 (2003).